35th Annual International Conference of the IEEE EMBS
Osaka, Japan, 3 - 7 July, 2013

Noise Behavior of MR Brain Reconstructions Using Compressed Sensing

Yuqiong Ding[1,2], Leslie Ying[3], Na Zhang [1,2], and Dong Liang[1,2*] , *Member, IEEE*

Abstract—**Compressed sensing (CS) has demonstrated great potential to reconstruct high quality MR images from undersampled k-space data. However, successful application of CS in clinic is still limited by many factors. One of the key factors is that the noise behavior in CS reconstructions remains largely unexplored. The main objective of this work is to analyze the noise behavior of MR reconstructions using CS method with different reduction factors. Our work focuses on brain CS-MRI reconstructions using non-linear conjugate gradient (NLCG) solvers. After reconstruction, the noise behavior is characterized using the MP-Law method. The results show that the spatial noise distributed non-uniformly, and the noise variance from CS reconstruction increases with reduction factors. A kind of fitting model is given, which can be used to predict the noise behavior parameter for different reduction factors, and the noise amplification factor maps are shown to prove the denoising capability of CS reconstruction. The results provide a qualitative and quantitative understanding of the noise behavior in CS-MRI with different reduction factors.**

I. Introduction

Image quality is a prime consideration in the design, manufacture and operational management of diagnostic imaging system. Signal to noise (SNR) [1], one key image quality determinant, is a frequently used metric as the assessment standard of imaging techniques, image reconstruction methods and imaging sequence [2] in Magnetic Resonance Image (MRI). The poor SNR MR image may bring down the credibility of diagnosis results and lead to misdiagnosis. The key of calculating SNR is to find the noise behavior of image precisely. However, getting meaningful and precise noise measurements is challenging [1-2].

Among today's many clinical imaging techniques, MRI has a number of advantages, such as multi-parameter imaging and harmless to human body. However, the speed at which data can be collected in MRI is fundamentally limited by physical and physiological constraints [3-4]. Therefore, how to improve the imaging speed without degrading the image quality has been becoming the main driving force and core issue to promote the development of MRI technology. A wide-variety of strategies for accelerating MRI scan have been reported, many of which involve reducing the number of acquired *k*-space samples [5].

Early practice is to use one excitation acquisition sequence of the multiple rows of phase encoding to improve MR imaging speed, such as Echo Planar Imaging (EPI) [6], Steady-state Free Precession (SSFP) [7], and etc.. The analysis of noise behavior indicated that the images acquired by these methods have Gauss white noise with zero mean and the noise is uniformly distributed on the whole image [8-10]. Parallel imaging (PI) techniques based on multi-channel phased-array coil has become the popular technique in MRI scanner, including Sensitivity Encoding (SENSE) [3], Generalized Auto-calibrating Partially Parallel Acquisitions (GRAPPA) [11], and etc.. The noise distribution in PI is not uniform and can be described by the spatially varying geometry factor (g-factor) which depends on parameters such as the coil geometry, phase-encoding direction, and acceleration factor [3]. The calculation of the g-factor leads to the fact PI is widely used in MR clinical medicine.

As a new mathematical framework for signal sampling and recovery, Compressed Sensing (CS) [12] has been widely applied in the field of biomedical imaging, especially in MRI [13]. The connection between CS theory and the undersampled MRI reconstruction problem was firstly made by Lusting et al. in [4], and then by more and more researchers. However, CS-related methods for MRI have not been adopted widely in the clinical setting due to their computational complexity, the uncertainty about which specific models (i.e. parameterizations, sparsifying transforms, and/ or numerical methods) to use, and mostly because that their performance has still not been extensively characterized [5]. To our best knowledge, the denoising capability of CS-based method has been demonstrated before only from reconstructions visually [4]. However, very little work was put in the quantitative and qualitative evaluation of the actual noise behavior using CS techniques, besides the quantitative evaluation of CS reconstructions in terms of sensitivity to reconstruction parameters as well as to the acquisition strategy for time-of-flight angiography data acquired on a 7T clinical MR scanner [14]. In summary, there is no evaluation such as noise

*This work is supported in part by the National Natural Science Foundation of China (61102043, and 8112010801), and the Basic Research Program of Shenzhen (JC201104220219A).

Yuqiong Ding, Na Zhang and Dong Liang are with Paul C. Lauterbur Research Center for Biomedical Imaging, Shenzhen Institutes of Advanced Technology, Chinese Academy of Sciences (e-mail: yq.ding@siat.ac.cn, na.zhang@siat.ac.cn, dong.liang@siat.ac.cn, phone +86-755-86392243).

Yuqiong Ding, Na Zhang and Dong Liang are with Key Laboratory of Health Informatics, Chinese Academy of Sciences, Shenzhen, Guangdong, China (e-mail: yq.ding@siat.ac.cn, na.zhang@siat.ac.cn, dong.liang@siat.ac.cn, phone +86-755-86392243).

Leslie Ying is with the Department of Biomedical Engineering and Department of Electrical Engineering,University at Buffalo, Buffalo, New York, United States (e-mail: leiying@buffalo.edu).

map or noise level to illustrate the noise behavior in CS reconstructions.

In this work, we aim to use a noise analysis method called MP-Law method [10] to analysis the noise behavior of MR reconstructions using CS method with different reduction factors. The work focuses on brain CS-MRI reconstructions using non-linear conjugate gradient (NLCG) solvers (SparseMRI [4]). The results provide a qualitative and quantitative understand of the noise behavior in CS-MRI with different reduction factors.

II. METHODOLY

A. Compressed Sensing in MRI

The CS method requires that: (a) the desired image has a sparse representation in a known transform domain (such as wavelet transform, discrete cosine transform, etc.), (b) the artifacts due to *k*-space undersampling are incoherent/noise-like (c) a nonlinear reconstruction can be used to enforce both sparsity of the image representation and consistency with the acquired data [4]. In MRI, the sampled linear combinations are simply individual Fourier coefficients (called *k*-space samples). We chose the NLCG solvers (SparseMRI [4]) as our CS reconstruction algorithm in this work.

The MR image can be reconstructed by solving the following optimization problem[4]:

$$\min \ \left\|\Psi \mathrm{m}\right\|_1 + \lambda TV(\mathrm{m}) \ s.t. \ \left\|\mathrm{F}_u \mathrm{m} - \mathrm{y}\right\|_2 < \varepsilon \quad (1)$$

where m denotes the reconstructed image, y is the measured *k*-space data from the scanner, ε controls the fidelity of the reconstruction to the measured data, Ψ denotes the linear operator that transforms from pixel representation into a sparse representation (e.g. wavelet transform), and F_u is the undersampled Fourier transform, $TV(\mathrm{m})$ is a TV penalty (finite-differences), and λ trades Ψ sparsity with finite-differences sparsity.

B. MP-Law Method

The MP-Law noise analysis method was developed by Ding et al. [10], which uses the statistical probability density function (PDF) of the KLT eigenvalues to distinguish random noise from signal. Specifically, a series of M dynamic images, each containing N pixels, can be represented by a $M \times N$ data matrix A. Let the covariance matrix of A be given by

$$A_{CM} = AA^T / N$$

where A^T is the transpose of A. There exists lower rank r ($r < M$) such that the remaining $M-r$ eigenvalues of A_{CM} will have a PDF that follows the MP distribution

$$p(\lambda) = \frac{1}{2\pi\alpha\sigma^2\lambda}\sqrt{\max(0,(\lambda_+ - \lambda)(\lambda - \lambda_-))} \quad (2)$$

where

$$\lambda_\pm = \sigma^2(1 \pm \sqrt{\alpha})^2 \quad \alpha = (M-r)/N \quad (3)$$

σ^2 is the mean noise variance of A, which equals the average of the last $M-r$ eigenvalues of A_{CM} and denoted by noise-level. Here #noise-only is used to denote the $M-r$ eigenvalues. Note that when the noise matrix contains non-IID noise that usually occurs with spatial image filtering or with PI techniques, N in Eq. (3) is reduced to a value (denoting as N -change) smaller than the number of image pixels [10]. In order to determine the optimal #noise-only and N -change, the Kolmogorov-Smirnov test (KS-test) was used. The goodness of fit (GOF) is optimized when there is minimum difference between the target PDF, as described by Eq. (2), and the empiric eigenvalues cumulative distribution function (CDF) from A_{CM} of a given image series using KS-test. Finally the *P* value can be obtained. Therefore, we can use the parameters such as #noise-only, N -change, noise-level, and *P* value to describe the noise behavior of reconstructions.

C. Brain CS-MRI with NLCG experiments

Five-slice, 100-times per slice, sequential, 2D FLASH image series of the brain were acquired on a 3T scanner (MAGNETOM Trio, SIEMENS, Erlangen, Germany) using an 12-channel head coil array for three healthy volunteers. The volunteers were requested to hold still during the acquisition. Informed consent was obtained from all volunteers in accordance with the institutional review board policy. The imaging parameters were: acquired matrix $= 128 \times 128$, slice thickness=5.0 *mm,* flip angle $= 70^\circ$, echo time= 3.08 *ms,* repetition time=100 *ms,* bandwidth=340 *Hz/pixel.* The full k-space data associated with each slice were retrospectively undersampled by a 2-D variable-density random undersampling mask. Examples of *R*=1 (no acceleration), *R*=3 and *R*=6 are illustrated in Figure 1 (a-c) respectively. The images were reconstructed by NLCG algorithm (SparseMRI [4], Eq. (1)) from undersampled Cartesian *K*-space with reduction factors *R* from 2 to 10.

To make the problem simple and get the solid conclusion, the weight for Ψ was set to zero. The reconstructions were conducted using several TV weights and chose the best one. For each volunteer, we have 5×9 reconstructed image sequences (100 images per sequence). After reconstruction, the noise behavior was characterized using the MP-Law method by identifying the noise-only eigenimages. The spatial noise, noise variance maps and one kind of fitting curve were acquired for each dataset. Then we predicted the noise-level for *R* = 12 and 14 using the model obtained from the results of *R*=2 to10. Additionally, the noise amplification factor (NA-factor), which is equivalent to g-factor [3], was calculated by $\sigma_R/(\sigma_F\sqrt{R})$, where σ_R^2 and σ_F^2 are noise variances (noise-level) calculated from the reconstructions of reduced and full data, respectively, using the MP-Law method. We use "NA-factor" to denote this value for

simplicity. The positions with "NA-factor" < 1 were colored to indicate the region where CS reconstruction can suppress noise.

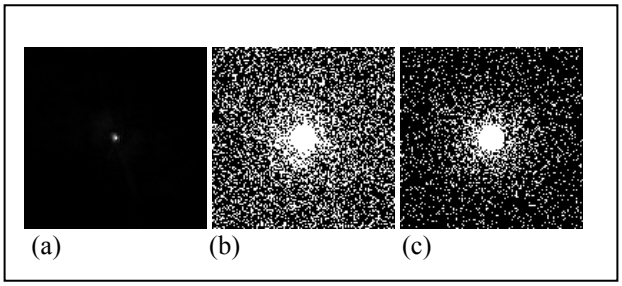

Figure 1. Example 2-D variable-density random sampling maps for (a) *R*=1 (b) *R*=3 and (c) *R*=6.

III. RESULTS

Table 1 illustrate the numerical results of one dataset of a volunteer with reduction factors *R* from 2 to 10, including fit probability *P* value, #noise-only, N -change and noise-level. As can be seen, the #noise-only and noise-level become higher with the increasing reduction factors, with the N -change becoming smaller. Particularly, when the reduction factor varying from 2 to 3, the noise-level increases sharply. But when the reduction factor is larger, the #noise-only and noise-level increase smoothly and tend to be constant. All of fitting probability is larger than 0.995.

Figure 2 shows the CS reconstructions, corresponding spatial noise maps, noise variance maps and the colored "NA-factor" maps (from up to bottom) of one dataset of one volunteer with reduction factors *R* from 2 to 10 (from left to right). The maps in the same category are shown on the same scale for different reduction factors (see the color bars). When *R* becoming larger, there are visible artifacts in the reconstructions. It is seen that firstly the spatial noise distributed non-uniformly in whole image area. Secondly, the noise variance in CS reconstructions presents spatially variant with high variance presents in outer boundary and then spreads to inner region with increasing reduction factors. Finally, the noise variance (noise-level) from CS reconstruction increases with reduction factors, which is consistent with the numerical results shown in the Table I. These may due to nonlinearly reconstructing from undersampled data, and the image-content-dependent constraint (image is transform sparse) used in CS reconstruction.

From the "NA-factor" maps shown on scale of [0.3855, 8.0637] in the last row of Fig. 2 (A), the noise amplification on the edge is more significant than that at the inner region. In order to quantatively demonstrate the denoising capability of CS, the colored noise-suppressed region ("NA-factor" <1) were shown on color scale of [0.3855, 1] in Fig. 2 (A). It can be seen that when R < 6, the noise-suppressed region shrinks with the increasing of R, and then expands when R increases from 6 to 10. This may be because that σ_R^2 increases slower than $\sqrt{R}$ in heavily undersampling scenario. And the Fig. 2 (B) shows the number of where NA-factor<1 for *R* from 2 to 10, and the numerical results agree with the colored map in Fig. 2 (A).

TABLE I. The numerical results of one datasets of one volunteere with reduction factors *R* from 2 to 10

	P value	#noise only	N change	noise-level
R = 2	0.999	63	3100	0.0007467
R = 3	0.999	70	2200	0.0016579
R = 4	0.999	74	1750	0.0025736
R = 5	0.999	76	1600	0.0032878
R = 6	0.997	77	1400	0.0033923
R = 7	0.996	78	1200	0.0033295
R = 8	0.996	79	1150	0.0033486
R = 9	0.996	79	1050	0.0033633
R = 10	0.995	79	950	0.0033764

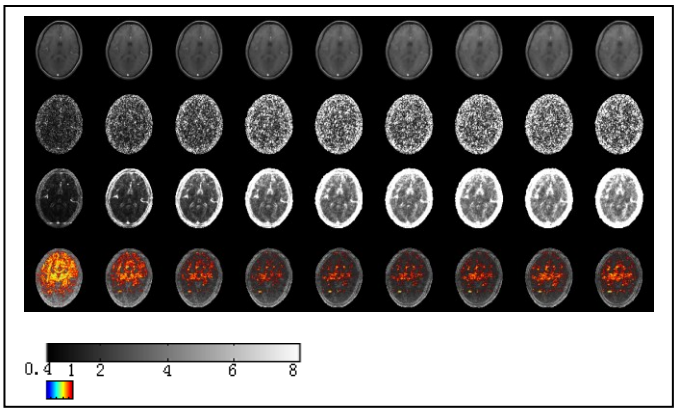

(A)

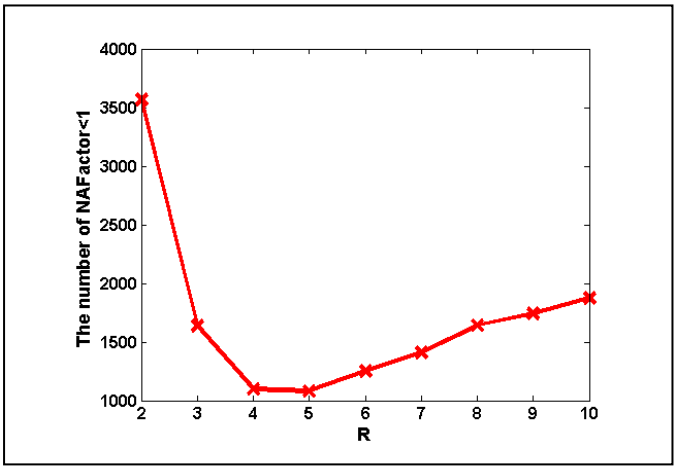

(B)

Figure 2. (A) The CS reconstructions, corresponding spatial noise maps, noise variance maps and the colored NA-factor maps (from up to bottom) of one dataset of one volunteer with reduction factors *R* from 2 to 10 (from left to right) (B) The number of where NA-factor<1 for *R* from 2 to 10

A fitting curve on noise-level versus reduction factor *R* for one image sequence is shown as in Figure 3, using the corresponding values with reduction factors R from 2 to 10 by step 1 (9 nodes, the curve is denoted by 9-curve). The model conforms to

$$noise-level = 0.009406(1-e^{-0.5983R}) - 0.005923$$

and the $R^2 = 0.9892$

In the Table II, we outline the predicting values of the #noise-only, N -change and noise-level using the fitting 9-curve models for *R* equals 12 and 14 for one slice of one volunteer, including the values from MP-Law method V_{true}, the predicting values V_{pre} ,the absolute values between V_{true} and V_{pre} (Error), and the error-level obtained by $\frac{|V_{pre}-V_{true}|}{V_{true}} \times 100\%$. It can be seen that the all error-level values for 9-curve models are controlled in less than 3%.

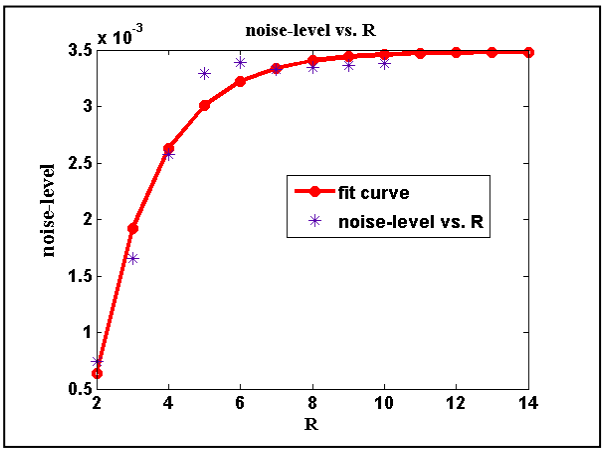

Figure 3. Fitting 9-curve of noise-level versus reduction factor *R* of one dataset of one volunteer using the corresponding values with reduction factors *R* from 2 to 10

TABLE II. The predicting results of a dataset of one volunteer

	noise-level	
	V_{true}	V_{pre}
R = 12	0.0033982	0.0034759
R = 14	0.0034041	0.0034809
	Error	**EL**
R = 12	0.0000777	2.3%
R = 14	0.0000768	2.3%

IV. CONCLUSION

In this work, the noise behavior with different reduction factors in CS brain reconstruction was analyzed by using the MP-Law method. Specifically, the NA-factor maps which demonstrate the denoising capability of CS were outlined. The results provide a qualitative and quantitative understanding of the noise behavior in brain CS-MRI, and will accelerate application of CS in clinical practice.

ACKNOWLEDGMENT

The authors would like to thank Guanghua Song for her help on the figures.

REFERENCES

[1] J. P. Wilde, J. A. Lunt, K. Straughan, "Information in magnetic resonance images: evaluation of signal, noise and contrast," *Medical & Biological Engineering & Computing*, 1997, vol. 35, pp. 259-265.

[2] P. Kellman, E. R. McVeigh, "Image reconstruction in SNR units: A general method for SNR measurement," *Magnetic Resonance in Medicine,* 2005, vol. 54, pp. 1439-1447.

[3] K. P. Pruessmann, M. Weiger, M. B. Scheidegger, P. Boesiger, "SENSE: sensitivity encoding for fast MRI," *Magnetic Resonance in Medicine,* 1999, vol. 42, pp. 952–962.

[4] M. Lustig, D. L. Donoho, J. M. Paul, "Sparse MRI: the application of compressed sensing for rapid MR imaging," *Magnetic Resonance in Medicine,* 2007, vol. 58, pp. 1182-1195.

[5] J. D. Trzasko, Z. H. Bao, A. Manduca, K. P. McGee, M. A. Bernstein, "Sparsity and los-contrast object detectabilty," *Magnetic Resonance in Medicine,* 2012, vol. 67, no. 4, pp. 1022-1023.

[6] I. S. Syed, D. Feng, S. R. Harris, M. W. Martinez, A. J. Misselt, J. F. Breen, D. V. Miller, P. A. Araoz, "MR Imaging of Cardiac Masse," *Magnetic Resonance Imaging Clinic,* 2008, vol. 16, no. 2, pp. 137-64.

[7] V. S. Lee, D. Resnick, J. M. Bundy, O. P. Simonetti, P. Lee, J. C. Weinreb, "Cardiac function: MR evaluation in one breath hold with real-time true fast imaging with steady-state precession," *Radiology,* 2002, vol. 222, pp. 835-842.

[8] R. M. Henkelman, "Measurement of signal intensities in the presence of noise in MR images," *Medical Physics,* 1985, vol. 12, no. 2, pp. 232-233.

[9] L. Kaufman, D. M. Kramer, L. E. Crooks, D. A. Ortendahl, "Measuring signal-to-noise ratios in MR imaging," *Radiology,* 1989, vol. 173, pp. 265-267.

[10] Y. Ding, Y. C. Chung, O. P. Simonetti, "A method to assess spatially variant noise in dynamic MR image series," *Magnetic Resonance in Medicine*, 2010, vol. 63, pp. 782-789.

[11] M. A. Griswold, P. M. Jakob, R. M. Heidemann, M. Nittka, V. Jellus, J. Wang, B. Kiefer, A. Haase, "Generalized autocalibrating partially parallel acquisitions (GRAPPA)," *Magnetic Resonance in Medicine,* 2002, vol. 47, pp. 1202–1210.

[12] D. L. Donoho, "Compressed sensing," *IEEE Transaction Information Theory,* 2006, vol. 52, pp. 1289-1306.

[13] W. T. Yin, S. Osher, D. Goldfarb, J. Darbon, "Bregman iterative algorithms for L1-minimization with applications to compressed sensing," *SIAM Journal on Imaging,* 2008, pp. 1-24.

[14] J. Milles J, J. M. Versluis, A. G. Webb, J. Reiber, "Quantitative evaluation of compressed sensing in MRI: application to 7T time-of-flight angiography," *In proceedings of IEEE/EMBS Region 8 International Conference on Information Technology and Applications in Biomedicine (ITAB),* 2010, pp. 1-4.

[15] K. Khare, C. J. Hardy, K. F. King, P. A. Turski, L. Marinelli, "Accelerated MR imaging using compressive sensing with no free parameters," *Magnetic Resonance in Medicine* , 2012, vol. 68, no. 5, pp. 1450-1457.